HHS Public Access

Author manuscript

Sleep Med. Author manuscript; available in PMC 2018 May 21.

Published in final edited form as:

Sleep Med. 2011 December ; 12(10): 966–974. doi:10.1016/j.sleep.2011.08.004.

Patterns in Pharyngeal Airflow Associated with Sleep-Disordered Breathing

Nelson B. Powell, MD, DDS, FACS[1,*], **Mihai Mihaescu, PhD**[2], **Goutham Mylavarapu, BTech**[2], **Edward M. Weaver, MD, MPH**[3], **Christian Guilleminault, MD, DM, DBiol**[4], and **Ephraim Gutmark, PhD, DSc**[5]

[1]Stanford University School of Medicine, Dept of Otolaryngology and Division of Sleep Medicine

[2]University of Cincinnati, School of Aerospace Systems

[3]University of Washington VAPSHCS 112, Department of Otolaryngology Head and Neck Surgery

[4]Stanford University School of Medicine Division of Sleep Medicine

[5]University of Cincinnati School of Medicine Department of Otolaryngology-Head and Neck Surgery, and School of Aerospace Systems

Abstract

Objective—To establish the feasibility of a noninvasive method to identify pharyngeal airflow characteristics in sleep-disordered breathing.

Methods—Four patients with sleep-disordered breathing who underwent surgery or used positive airway pressure devices and four normal healthy controls were studied. Three-dimensional CT imaging and computational fluid dynamics modeling with standard steady-state numerical formulation were used to characterize pharyngeal airflow behavior in normals and pre-and post-treatment in patients. Dynamic flow simulations using an unsteady approach were performed in one patient.

Results—The pre-treatment pharyngeal airway below the minimum cross-sectional area obstruction site showed airflow separation. This generated recirculation airflow regions and enhanced turbulence zones where vortices developed. This interaction induced large fluctuations in airflow variables and increased aerodynamic forces acting on the pharyngeal wall. At post-treatment, for the same volumetric flow rate, airflow field instabilities vanished and airflow characteristics improved. Mean maximum airflow velocity during inspiration reduced from 18.3±5.7 meters/second pre-treatment to 6.3±4.5 meters/second post-treatment ($p=0.002$), leading to a reduction in maximum wall shear stress from 4.8±1.7 Pascals pre-treatment to 0.9±1.0 Pascals post-treatment ($p=0.01$). The airway resistance improved from 4.3±1.4 Pascals/Liter/minute at pre-treatment to 0.7±0.7 Pascals/Liter/minute at post-treatment ($p=0.004$). Post-treatment airflow characteristics were not different from normal controls (all $p\geq0.39$).

[*]Request for reprints: Corresponding Author: Nelson Powell MD, DDS, FACS, 6 Knoll Vista, Atherton, CA 94027, nelsonpowell@sbcglobal.net, Phone (650) 328-0511.

Conclusion—This study demonstrates that pharyngeal airflow variables may be derived from CT imaging and computational fluid dynamics modeling, resulting in high quality visualizations of airflow characteristics of axial velocity, static pressure and wall shear stress, in sleep-disordered breathing.

Keywords

Sleep-disordered breathing; Obstructive sleep apnea; Computational fluid dynamics; Pharyngeal airflow and airway dynamics; Axial velocity; Static pressure; Wall shear stress; Vibratory tissue damage

Introduction

Sleep-disordered breathing (SDB) is a disorder of disrupted upper airway airflow during sleep, due to anatomic constrictions and sleep-related collapsibility. Management of SDB has historically focused on treatment of the anatomic upper airway[1]. Little attention has been given to airflow characteristics of the pharyngeal airway in SDB which might have localized airflow and tissue effects that could be future targets of therapy.

Investigators have previously suggested that tissue vibration and snoring may cause damage to the soft tissues, vessels and nerves[2-4] which in turn may exacerbate SDB. Although the metrics of vibration and snoring have been studied, they seldom have been correlated with airflow effects, which may play a role in airway collapsibility. Our overarching question is "Do the pattern and characteristics of pharyngeal airway airflow have an important role in the etiology of SDB?" Our immediate question for this feasibility study is, "Can pharyngeal airflow be objectively evaluated?" This proof of concept and feasibility study was designed utilizing Computed Tomography (CT) and Computational Fluid Dynamics (CFD) modeling[5-7].

CFD has been increasingly used to assess upper airway anatomy and airflow, and to explore virtual reality surgery in SDB[8-12]. However, seldom has CFD been specifically applied to distinguish between pharyngeal airflow characteristics at pre and post-treatment conditions. CFD and imaging metrics permit spacial visualization of the three-dimensional (3D**)** airflow in the upper airway. Within the generated virtual airway model airflow data are calculated from which variables of interest such as flow axial velocity, static pressure, wall shear stress (WSS), and airway resistance can then be extracted. The purpose of this feasibility study was to demonstrate the use of this noninvasive approach to model pharyngeal airflow and airway characteristics in normal controls and SDB patients before and after treatment. Future studies may use these techniques to test hypotheses about sleep-related airway collapsibility and the effects of therapy in SDB.

Methods

Subjects

Control subjects were selected prospectively from normal healthy people who reported no snoring or excessive daytime sleepiness (Table 1). The patients were selected retrospectively from subjects with moderate or severe SDB. They were successfully treated with either

maxillo-mandibular advancement (MMA) surgery or positive airway pressure (PAP) therapy. Both MMA patients had previously undergone Phase 1 surgery (uvulopalatopharyngoplasty and genioglossus advancement), but still had moderate or severe SDB prior to MMA as shown by the polysomnography (PSG) characteristics in Table 2. The pre and post-treatment data were collected as part of our standard work-up and follow-up. The study period was from May 2008 to January 2010. Each participant provided informed consent. The usage of de-identified data for research was approved by the Stanford University Institutional Review Board.

Polysomnography

Clinical evaluation and attended overnight PSG were part of the pre and post-treatment evaluations for the SDB subjects. PSG included the following variables: electroencephalogram (4 derivations), electro-occulogram (2 derivations), chin and leg electromyogram, electrocardiogram modified V2 lead, finger plethysmography, body position, neck microphone, nasal cannula pressure transducer, oral thermistor, uncalibrated inductive plethysmography thoracic and abdominal bands, pulse oximetry, and transcutaneous carbon dioxide. PSG results are listed in Table 2.

Functional imaging and airway reconstruction

All SDB patients underwent pre and post-treatment 3D-CT imaging using a NewTom 3G Cone Beam CT scanner with an average 6.5 seconds exposure time at end expiratory breathing while lying supine and awake in a neutral head (Frankfort plane) position. The average energy used: 110 Kilovolt peak (KVP), between 6-11 milliampers (MA) varies based on patient size. For all four controls the 3D-CT imaging and CFD airway modeling were applied using the same study protocol as for the SDB patients. Patients treated with PAP used their equipment at the prescribed pressures and bypassing ramping. The 12” scan was formatted at 0.4 millimeters slice thickness. Pre and post-treatment models were reconstructed from the level of the nasal choanae (top-face of the computational domain) to the base of the epiglottis (bottom-face of the computational domain) using the CTs and the medical-imaging-software MIMICS® (Materialise, Belgium). The procedure involved grouping voxels in the Hounsfield Units (HU) range of interest (≈ −1000HU) into a mask from which, by surface triangulation the raw 3D model was generated. This was then exported into a remesher where the individual faces of the airway (i.e. top, bottom, and wall surfaces) were demarcated and the mesh quality at the surfaces was improved. Using the CFD pre-processor GAMBIT (Ansys®, USA) the unstructured tri/tetrahedral hybrid mesh within the airway volume was constructed. The maximum edge length for the mesh used in all RANS calculations is 0.0005m. The maximum edge length for the mesh used in LES calculations is 0.00035m and 0.0005m for Pre-op and Post-op cases, respectively. The maximum edge length for meshes used in LES calculations is based on the estimated Taylor micro-scale computed for the flow conditions investigated. Figure 1 shows the pre and post-treatment CT scans and reconstructed airway models for subject #5 (MMA).

Pharyngeal airflow modeling

The commercial CFD software FLUENT (Ansys®, USA) was used to solve the flow governing equations and to calculate the distributions of the flow variables (velocity,

pressure, and wall shear stress) in each of the generated pharyngeal airway models. Within the CFD framework the steady-state Reynolds Averaged Navier-Stokes (RANS) with correspondent turbulence closures is the most popular formulation used to model respiratory flows[13-16]. With adequate tuning of the empirical constants RANS can provide accurate time averaged data for a particular flow field[17]. It is robust and rapid but only in terms of time-averaged quantities but cannot predict the flow field dynamics. However, it allows a fast screening of the airway models to obtain valuable mean data about airflow and airway resistance. The steady-state RANS formulation with the k-ω shear stress transport (SST) turbulence model[18] was applied for all subjects, being preferred to other models due to its superiority both in the treatment of the viscous near-wall region and in its accounting for the effects of adverse pressure gradient[17, 18]

An increased level of detail and accuracy for unsteady, separated or vortical turbulent flows are provided by the more complex and time-intensive use of the unsteady Large Eddy Simulation (LES) approach[19]. The LES was used only as a single “trial” for subject *#5* to calculate the inspiratory and expiratory pharyngeal flows and to compare to the RANS parameters. The purpose was to examine the feasibility, the quality and the level of detail of the flow data and the unique features associated with LES. The computational time for running a RANS simulation on a single processor was up to eight hours, while an unsteady LES calculation took approximately ten days. Hence, the LES was applied only to subject #5.

Numerical methods and boundary conditions

The incompressible flow governing equations were discretized on the computational domain using second-order finite-volume schemes. For the time integration, a second-order implicit scheme was employed. The coupling between the velocity and pressure fields was realized using the SIMPLE algorithm[20]. The WALE Subgrid-Scale model was used with the LES calculations. The boundary conditions consisted in axial velocity specification at the inlet plane to match the desired volumetric flux, no-slip boundary conditions for velocity at the airway wall, and a flux-conserving zero-gradient condition at the outlet surface of the computational domain.

Two different validation studies[7,22] were completed by our group to show that the CFD formulations used here (i.e. RANS with k-ω SST model and LES approach) are the most suitable to be used when analyzing upper respiratory airflows. Both studies showed very good agreements between computational and experimental data in terms of wall static pressures and flow velocities as presented in Appendix A.

Results

Steady-state flow simulations

The RANS k-ω SST formulation was used to simulate airflows for all subjects, including pre-treatment and post-treatment for SDB patients, during both inspiration and expiration phases at peak flow rates of 30 liters per minute (L/min).The obtained data in terms of

maximum velocity, WSS, minimum wall static pressure, and pharyngeal airway resistance are summarized in Table 3.

Contours of the axial velocity (m/sec), wall static pressure (Pascal), and WSS (Pascal) for pre and post-treatment conditions during inspiration are shown for subject #5 in Figures 2 and 3 respectively.

For *pre-treatment* conditions (Figure 2) the flow accelerated at zone 2 where the crosssectional area (CSA) was at a minimum. Downstream of it the velocity decelerated corresponding to the increased airway CSA. The flow also separated from the wall, producing a jet that impinged on the anterior airway downstream of zone 3, but above the tip of the epiglottis (zone 4). A recirculation region (negative velocities) was formed on the anterior wall of the airway (zone 3) below the minimum CSA. A second acceleration of the flow occurred near zone 4, where the retroflexed epiglottis became a constriction point. These complex flow patterns appear, in part, to result from the anterior wall shape with abrupt changes in CSA that induced flow separation.

The regions with the high axial velocities, zones 2 & 4 in Figure 2 were characterized by the largest negative wall static pressure values of −134 Pascals (Pa) and −160 (Pa) respectively. The location where the jet impinged on the wall experienced increased pressure. Maximum WSS values were observed at zones 2 & 4 due to the higher velocity and the increased friction between the flow and the airway lumen at these regions. Increased shear was also apparent at the location where the jet impinged on the anterior wall between zones 3 & 4. The distribution of velocity, pressure, and shear stress at each cross section was not uniform around the circumference of the airway.

For the *post-treatment* condition, Figure 3, the overall increase in the airway CSA corresponded to a decrease in the magnitude of the flow velocity when compared with the pre-treatment case. The removal of abrupt cross-sectional changes, in particular between zones 1 & 4, yielded smoother flow without the severe separation from the walls. The flow started accelerating only at the tip of the epiglottis (downstream of zone 4) where the CSA was reduced. The maximum velocity reached post-treatment was approximately 5m/sec compared to 13.3m/sec for the pre-treatment case. The post-treatment wall static pressure minimum in the retropalatal region was only −9Pa compared to the pre-treatment value of −134Pa. This is important since the induced negative wall static pressure loads caused at the regions with flow acceleration lead to forces of adduction which if large enough may predispose airway to collapse. The maximum WSS value was reduced by 70% post-treatment.

The large variations in the pre-treatment flow variables as compared with the post-treatment ones are also emphasized in Figure 4. The data are presented in terms of maximum velocity magnitude along the pharyngeal airway length (z), with wall static pressure and shear stress distributions along the anterior wall in the mid-sagittal plane of the airway model. Similar observations were made for the other SDB subjects (Table 3).

Treatment outcome evaluation

Comparisons of pertinent flow parameters (maximum velocity, WSS, minimum wall static pressure and airway resistance) are presented for each control subject and patient (pre and post-treatment) in Table 3. Post-treatment values were significantly improved compared to pre-treatment in the treated SDB patients (all $p \leq 0.028$), and post-treatment values were in average similar to the normal control subject values (all $p > 0.39$). The resistance of the airway is defined as ($R=\Delta P/Q$), with the pressure drop (ΔP) in Pascals and the flow rate (Q) in L/min. The computed airway resistances were significantly improved after treatment, both during inspiration and expiration (both $p < 0.02$). This was in agreement with the fact that the treatments resulted in an increase of the pharyngeal *airway volume* by 120±70%. Moreover, the increase in cross-sectional area of the retro-palatal post-treatment leaded to significant increase of the *wall static pressures at the maximum narrowing.* Accordingly, the aerodynamic forces generated at pre-treatment by the negative wall pressure loads that could potentially lead to airway collapse are drastically reduced after treatment. Significant reductions of *maximum WSS* values were found as well. These airflow improvements are in agreement with the corresponded PSG findings after treatment.

LES results

To capture the airflow dynamics along the pharyngeal airway, the LES approach for subject #5 demonstrate its potential advantages of using LES. The LES calculations were performed for the peak inspiratory and expiratory flow rates of 30L/min for a period of roughly 50 flow-through times, achieving a converged solution at each time-step ($\Delta t = 0.000025$sec). Unlike the steady-state RANS computations, the LES results describe the dynamic variation of the flow field as a function of time such that instantaneous flow field information is available at any time instance. Snapshots of pre-treatment instantaneous axial velocity and WSS values calculated at two different time instances during inspiration for subject #5 are shown in Figures 5 and 6. The axial velocity (m/sec) distribution in Figure 5 presented in the sagittal plane through the airway show that a jet is formed at the minimum CSA and at its edges (shear layers) vortices are initiated by jet instabilities. These vortices are convected downstream by the jet flow and are impinging on the anterior airway wall. In the second time instance shown, the jet is deflected away from the anterior wall towards the posterior side. These instabilities in the flow field observed between zones 3 and 4 occur over 400 times per second as shown in Appendix B. The jet flow separated from the airway wall immediately downstream of the minimum CSA, generating a strong recirculation zone at the space between the jet and the anterior airway wall. The dynamics of this recirculation bubble can be observed by following the movement of the negative velocity region from the first to the second time-frame in Figure 5. These fluctuations in the motion of the recirculation bubble occur over 30 times per second (Appendix B).

Because of these two phenomena (flapping jet and recirculation) the aerodynamic forces (pressure and shear) induced by the flow on the airway lumen at these locations fluctuate and change from one time-instance to the other. This caused fluctuations in the WSS as shown in Figure 6 particularly in the regions where the jet impinges on the wall and where the flow recirculates.

The time-averaged results obtained for subject #5 from LES were compared to the RANS data as summarized for maximum velocity, WSS, static pressure, and airway resistance in Table 4. While the maximum velocity results are comparable, the WSS and resistance are different for some cases.

Discussion

This investigation based on functional imaging and CFD was performed to observe airflow patterns in normal controls and SDB patients at pre and post-treatment. The results demonstrated that flow patterns and flow variables can be successfully determined in the pharyngeal airway by the use of CFD modeling. The pharyngeal airflow characteristics (axial velocity, wall static pressure, and WSS) were quantified and as compared with the pre-treatment state, a clear improvement in airway resistance after treatment was observed. Moreover, the post-treatment flow characteristics appeared similar to normal controls and were in agreement with the dramatic improvements seen in the post-treatment polysomnography data.

Airway zones with reduced static pressure may be more susceptible to collapse. Increased WSS and high frequency shear stress variations induced by jet impingement and reversed flow may possibly lead to tissue irritation and progressive damage. High and low frequency flow fluctuations at the airway wall due to jet flapping and recirculating separated flow that were demonstrated by LES (Appendix B) are likely to induce vibrations in the compliant airway lumen. The CFD methodology that is described here can be extended to calculate the interaction between the flow and the compliant airway wall by including movement of the airway wall due to pressure and shear stress forces that act on the wall. This improved method is known as Fluid-Structure Interaction (FSI). It can provide, in addition to airflow, pressure and WSS, also wall steady (collapsibility) and unsteady (vibrations) movement characteristics. This methodology could clarify airflow mechanisms of tissue vibration and snoring, and will enable investigation of tissue damage mechanisms in SDB. However, there are very few published papers that utilized this approach for computational studies in the upper airway.[23-26] Most published work used either simplified or two-dimensional airway models. The following are the main difficulties in employing this approach to the upper airway: 1) Availability of reliable data on the mechanical properties of soft-tissues surrounding the airway, such as Young modulus, Poisson’s ratio and density. The soft tissue properties are patient specific and are sensitive to awake or sleep conditions; 2) The reconstruction of soft tissue models surrounding the upper airway requires higher quality of MR images compared to that which is needed for reconstructing 3D airway (flow domain) models; 3) Discretization of three-dimensional flow and structure domains with perfect interface matching on either side. We are currently working on developing the techniques necessary for FSI.

Although our primary emphasis in this study was to evaluate characteristics of pharyngeal airflow in the airway, we also wished to expand our understanding of how airflow in SDB may interact with the airway walls. The following provides some aspects of this issue.

Paulsen et al[27] evaluated epithelial structural changes in SDB and reported progressive structural and mucosal changes caused by snoring which the researchers reported could be a factor in airway collapsibility. An interesting study by Wasserman et al[28] reported that vibration from daily power tools is seen in 8-10 million workers in America. Curry et al[29] noted that damage was so prevalent in humans it was called the hand-arm vibration syndrome (HAVS) and reported that vibration is known to cause neural and vascular dysfunctions. They used a Sprague-Dawley rat-tail artery model and evaluated arterial endothelial cells using electron microscopy and Laser Doppler surface recordings. Vibration over a very short period caused a vasoconstriction with a decrease in blood perfusion and subsequent damage to the arterial endothelium. Govindaraju et al[30] later reported that "continuous vibration invoked a persistent reduction in vascular lumen size". They postulated that patterns of vibration could influence the type of vibration injury. Although these citations in animals are not airflow related they are clearly associated with vibration, tissue alteration and damage. Lee et al[31] evaluated heavy snoring as a cause of carotid artery atherosclerosis independent of other risk factors. In Guilleminault et al[32] long term CPAP study, they found persistent neurological lesions despite treatment, which also raises a question of the airflow effects of CPAP itself. Lee et al[31] study on pharyngeal neuropathy concurs with the Christian Guilleminault study.

It is plausible that *unsteady airflows* may result in vibration and snoring which may cause high cycle tissue fatigue to the upper airway and exacerbate SDB. A recent investigation published in Sleep in 2011 reported that tissue vibration may have a role in inducing carotid artery endothelial dysfunction in SDB, Cho J, et al[33]

Discussion of Limitations

This feasibility study, although limited in numbers, has shown that pharyngeal airflow characteristics can be identified using objective advanced imaging and CFD. Several other limitations are noted in this study and are acknowledged. We recognize that there are limitations in being awake which is different from being asleep and the abnormalities that we note during wakefulness are those noted in "the best situation". This is important as in these "best situations" we were able to demonstrate abnormalities, such as those found in pharyngeal airflow characteristics at baseline.

Since our subjects were awake and static we studied each supine with great attention to place subjects in exactly the same head position using an equivalent of a cephaolstat, at second study, and subjects were thus comparable to each other in both before and after surgery. All imaging was done at a same time of day for each subject.

We also acknowledge the effects of neural compensatory reflexes as an important limitation in our study. However, these issues have been previously studied in experimental conditions. It is well known that when a patient presents with (AASM) defined OSA, even if with a low AHI, compensatory mechanisms are impaired with impairment of local sensory mechanisms. As shown by Dematteis et al[34] there may be a gradient of impairment when AHI is between 5 and 15 but impairment is already present at low AHI. Note that the majority of studies including the one performed by Dematteis were performed on subjects

that were awake. So some compensatory mechanisms may still be present in subjects with low AHI, it is probable that all OSA patients have impairment of neural compensatory mechanisms to a variable degree during wakefulness but no one to date has been able to appropriately quantify the degree of impairment during wakefulness. Hence, all OSA patients including ours, have impairment of neural compensatory mechanisms to a variable degree during wakefulness that was shown in previous published studies (Frieberg et al[2], Dematteis et al[34], Kimoff et al[35])

We further acknowledge that limitations of rigidity in imaging and modeling decrease the value of movement and compliance of the soft tissues of the SDB pharynx. However, for our investigation a non- collapsible modeling was only a modest underestimation step behind dynamic modeling. As technology improves for measuring the airway dimensions awake or asleep or the airflow dynamics of awake or sleep it should continue to improve our ability to model the airway and airflow in SDB.

It is clear that neurological impairment is at the bases of OSA. There may be limitations in this study concerning neurological impairments in the upper airway. However, in summary there are currently over fourteen peer reviewed international articles that indicate the presence of neural, vibratory and soft tissue impairment with local lesions in the upper airway. Testing in most of these studies was performed while the patients were awake. [2-4, 27-38]. It is important to indicate this neurological impairment in awake patients as our study is performed on awake subjects.

The research was not designed or expected to answer the question of whether airflow in the pharyngeal airway could result in airway tissue damage over time. However, inferentially, this work suggests a possible relationship between pharyngeal airflow characteristics in SDB, and a possible method for studying these relationships. We do not test these hypotheses in this feasibility study, but we propose them as working hypotheses toward future work.

Conclusion

This feasibility study supports the concept that flow modeling methods for pharyngeal airway airflow in SDB may be used in understanding the complicated pathophysiology of SDB. Further studies will be warranted to test the predictive value of these models on treatment effects with surgery, PAP or oral appliances.

Supplementary Material

Refer to Web version on PubMed Central for supplementary material.

References: Revision Clean Copy

1. Schwab R. Pro: Sleep apnea is an anatomic disorder. Am J Respir Crit Care Med. 2003; 168:270–273. [PubMed: 12888606]
2. Friberg D, Ansved T, Borg K, Carlsson-Nordlander B, Larsson H, Svanborg E. Histological indications of a progressive snorers' disease in an upper airway muscle. Ann J Respir Crit Care Med. 1998; 157:586–593.

3. Woodson BT, Garancis JC, Toohill RJ. Histopathologic changes in snoring and obstructive sleep apnea syndrome. Laryngoscope. 1991; 101:1318–1322. [PubMed: 1766303]
4. Namystowski G, Scierski W, Zembala-Nozynska E, Nozynska J, Misiolek M. Histopathologic changes of the soft palate in snoring and obstructive sleep apnea syndrome patients. Otolaryngol Pol. 2005; 59(1):3–19.
5. Cabalerro P, Alvarez-Sala R, Garcia-Rio F, Padros C, Hernan M, Villamor J, Alvarez-Sala J. CT in the evaluation of the upper airway in healthy subjects and in patients with obstructive sleep apnea syndrome. Chest. 1998; 113(1):111–116. [PubMed: 9440577]
6. Mihaescu M, Gutmark EJ, Murugappan S, Elluru R, Cohen A, Willging J. Modeling flow in a compromised pediatric airway breathing air and heliox. Laryngoscope. 2008; 118(12):2205–2211. [PubMed: 19029854]
7. Mylavarapu G, Murugappan S, Mihaescu M, Kalra M, Khosla S, Gutmark EJ. Validation of computational fluid dynamics methodology used for human upper airway flow simulations. J Biomech. 2009; 42:1553–1559. [PubMed: 19501360]
8. Vos W, De Backer J, Devolder A, Vanderveken O, Verhulst S, Salgado R, Germonpre P, Partoens B, Wuyts F, Parizel P, De Becker W. Correlation between severity of sleep apnea and upper airway morphology based on advanced anatomical and functional imaging. J Biomech. 2007; 40(10):2207–2213. [PubMed: 17178125]
9. Huang Y, White DP, Malhorta A. Use of computational modeling to predict responses to upper airway surgery in obstructive sleep apnea. Laryngoscope. 2007; 117:648–653. [PubMed: 17415135]
10. De Backer J, Vos W, Verhulst S, De Backer W. Novel imaging techniques using computer methods for the evaluation of the upper airway in patients with sleep-disordered breathing: a comprehensive review. Sleep Med Rev. 2008; 12:437–447. [PubMed: 18926741]
11. Mihaescu M, Murugappan S, Gutmark EJ, Khosla SM, Donnelly LF, Kaira M. Computational fluid dynamics analysis of upper airway reconstructed from magnetic resonance imaging data. Ann Otol Rhinol Laryngol. 2008a; 117:303–309. [PubMed: 18478841]
12. Mihaescu M, Murugappan S, Gutmark EJ, Donnelly LF, Kalara M. Computational modeling of upper airway before adenotonsillectomy for obstructive sleep apnea. Laryngoscope. 2008b; 118(2):360–362. [PubMed: 18043493]
13. Xu C, Sin S, McDonough JM, Udupa JK, Gucz A, Wootton DM. Computational fluid dynamics modeling of the upper airway of children with obstructive sleep apnea syndrome in steady flow. J Biomech. 2006; 39:2043–2054. [PubMed: 16098533]
14. Sung S, Jeong S, Yu Y, Hwang C, Pae E. Customized three-dimensional computational fluid dynamics simulation of the upper airway of obstructive sleep apnea. Angle Ortho. 2006; 76(5): 791–799.
15. Yu C, Hsiao H, Lee L, et al. Computational fluid dynamics study on obstructive sleep apnea syndrome treated with maxillomandibular advancement. J Craniofac Surg. 2009; 20:426–430. [PubMed: 19305244]
16. Jeong S, Kim W, Sung S. Numerical investigation on the flow characteristics and aerodynamic force of the upper airway of patients with obstructive sleep apnea using computational fluid dynamics. Med Eng Phys. 2007; 29:637–651. [PubMed: 17049904]
17. Wilcox, D. Turbulence modeling for CFD. La Canada (CA): DCW Industries; 1993. p. 117-125.
18. Menter F. Two-equation eddy-viscosity turbulence models for engineering applications. AIAA Journal. 1994; 32(8):1598–1605.
19. Pope, SB. Turbulent flows. New York: Cambridge University Press; 2000. p. 558-638.
20. Vandoormaal J, Raithby G. Enhancements of the SIMPLE method for predicting incompressible fluid flows. Numer Heat Transfer. 1984; 7:147–163.
21. Nicoud F, Ducros F. Subgrid-scale stress modeling based on the square of the velocity gradient tensor. Flow Turbul Combust. 1999; 62(3):183–200.
22. Mihaescu, M., Mylavarapu, G., de Luzan, C., et al. Large eddy simulation for estimating flow instabilities associated with obstructive sleep apnea in a pharyngeal airway. Int Conf on Jets, Wakes and Separated Flows. 2010. Available in URL http://www.ase.uc.edu/~files_/Mihaescu_Mihai_2OSA_ICJWSF10.pdf

23. Mylavarapu, G., Mihaescu, M., Murugappan, S., Gutmark, EJ., Kalra, M. Fluid Structure Interaction Analysis in Human Upper Airways to Understand Sleep Apnea. 48th AIAA Aerospace Science Meeting; January 2010; Orlando, Florida.
24. Balint TS, Lucey AD. Instability of a cantilevered flexible plate in viscous channel flow. Journal of Fluids and Structures. 2005; 20(7):893–912.
25. Payan Y, Pelorson X, Perrier P. Physical modeling of airflow-walls interaction to understand Sleep Apnea Syndrome. Surgery Simulation and Soft Tissue Modeling. 2003; 2673:261–269.
26. Chouly F, Van Hirtum A, Lagree PY, Pelorson X, Payan Y. Numerical and experimental study of expiratory flow in case of major upper airway obstructions with fluid- structure interaction. Journal of Fluids and Structures. 2008; 24(2):250–269.
27. Paulson F, Phillip P, Tsokos M, Jungmann K, Muller A, Verse T, Pirsig W. Upper airway epithelial structural changes in obstructive sleep-disoriented breathing. Am J Respir Crit Care Med. 2002; 166:501–509. [PubMed: 12186828]
28. Wasserman D, Badger D, Doyl L. Industrial vibration and overview. J Am Soc Safety Eng. 1974; 19:38–43.
29. Curry BD, Bain JL, Yan Ji-G, Zhang LL, Yamaguchi M, Matloub HS, Riley DA. Vibration injury damages arterial endothelial cells. Muscle Nerve. 2002; 25:527–534. [PubMed: 11932970]
30. Govindaraju SR, Curry BD, Bain JL, Riley DA. Comparison of continuous vibration effects on rat-tail artery and nerve. Muscle Nerve. 2006; 34(2):197–204. [PubMed: 16691604]
31. Lee SA, Amis TC, Byth K, Larcos G, Kairaitis K, Robinson TD, Wheatley JR. Heavy snoring as a cause of carotid artery atherosclerosis. Sleep. 2008; 31(9):1207–1213. [PubMed: 18788645]
32. Guilleminault C, Huang Y, Kirisoglu C, Chan A. Is obstructive sleep apnea syndrome a neurological disorder? A continuous positive airway pressure follow-up study. Ann Neurol. 2005; 58:880–887. [PubMed: 16240364]
33. Cho J, Witting P, Verma M, Wu B, Shana A, Kairaitis K, Amis T, Wheatly J. Tissue vibration induces carotid artery endothelial dysfunction: A mechanism linking snoring and carotid atherosclerosis? Sleep. 2011; 34(6):751–757. [PubMed: 21629363]
34. Dematteis M, Levy P, Pepin J-L. A simple procedure for measuring pharyngeal sensitivity: a contribution to the diagnosis of sleep apnea. Thorax. 2005; 60:418–426. [PubMed: 15860719]
35. Kimoff RJ, Sforza E, Champagne V, Ofiara L, Gendron D. Upper airway sensation in snoring and obstructive sleep apnea. Am J Respir Crit Care Med. 2001; 164:250–255. [PubMed: 11463596]
36. Amatoury J, Howitt L, Wheatley J, Avolio A, Amis T. Snoring-related energy transmission to the carotid artery in rabbits. J Appl Physiol. 2006; 100:1547–1553. [PubMed: 16455812]
37. Rice T, Strollo P, Commentary on Jin-Cho. et al. Tissue vibration induces carotid artery endothelial dysfunction: A mechanism linking snoring and carotid atherosclerosis? Sleep. 2011; 34(6):251–757. [PubMed: 21358841]
38. Sabato R, Guido P, Resta S, Spanevello A, Barbaro F. Airway inflammation in patients affected by obstructive sleep apnea. Monaldi Arch Chest Dis. 2006; 65:102–105. [PubMed: 16913581]

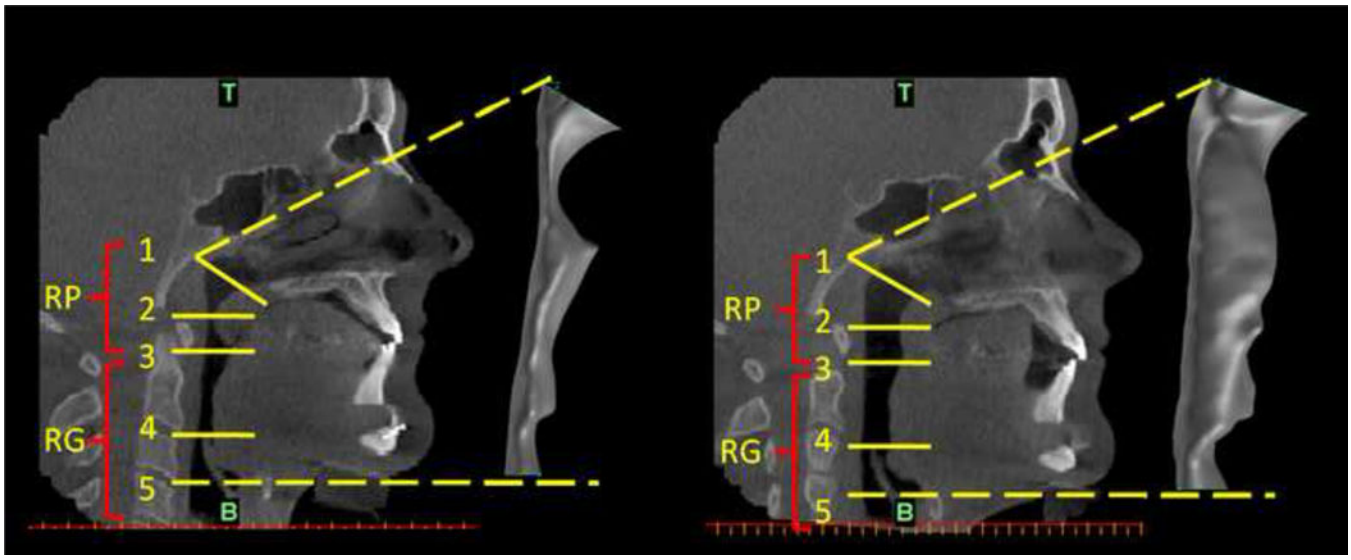

Figure 1.

SDB Patient #5: Pre-treatment and post-treatment CT sagittal views of the upper respiratory tract together with side views of the reconstructed airway models at pre and post-treatment conditions: pre-treatment CT image and pre-treatment reconstructed airway volume (left); post-treatment CT image and post-treatment reconstructed airway volume (right). The anatomical locations marked on the CT images with RP and RG refer to the retro-palatal and retro-glossal regions, while zones 1, 2, 3, 4, and 5 refer to: 1- nasal choanae level (T is top face of the computational domain); 2 - the minimum cross-sectional area (CSA) in the RP region at pre-treatment condition; 3 - tip of uvula; 4 - tip of epiglottis; 5 - base of epiglottis (B is bottom face of the computational domain).

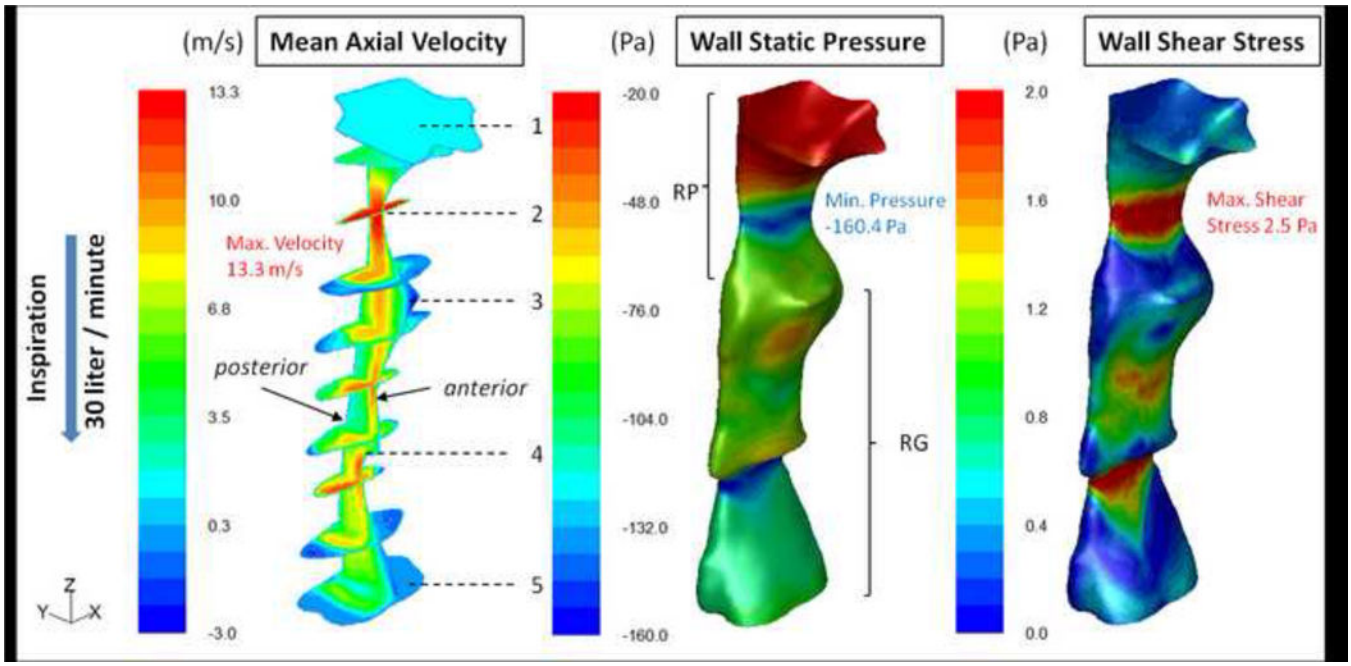

Figure 2.

SDB Patient #5: Pre-operative distributed contour values of three airflow variables, which from left to right respectively are: mean axial velocity (m/sec); mean wall static pressure (Pa) and wall shear stress (Pa). Calculations performed with steady-state RANS (k-ω SST model) during inspiration. The axial velocity field is shown inside the airway's volume using a sagittal mid-plane and ten cross-sectional planes. The numbering from 1 to 5 are area zones as in Figure 1. The static pressure and shear stress distributions are presented on the airway wall. The narrowest sites (behind the palate and epiglottis) correspond to the sites of maximum velocity (red area), minimum static pressure (greatest negative pressure, blue area), and maximum wall shear stress (red area). The coordinate system to the left of the color bar is used for orientation purposes; z-axis in the direction of the flow and x-axis in the anterior-posterior direction.

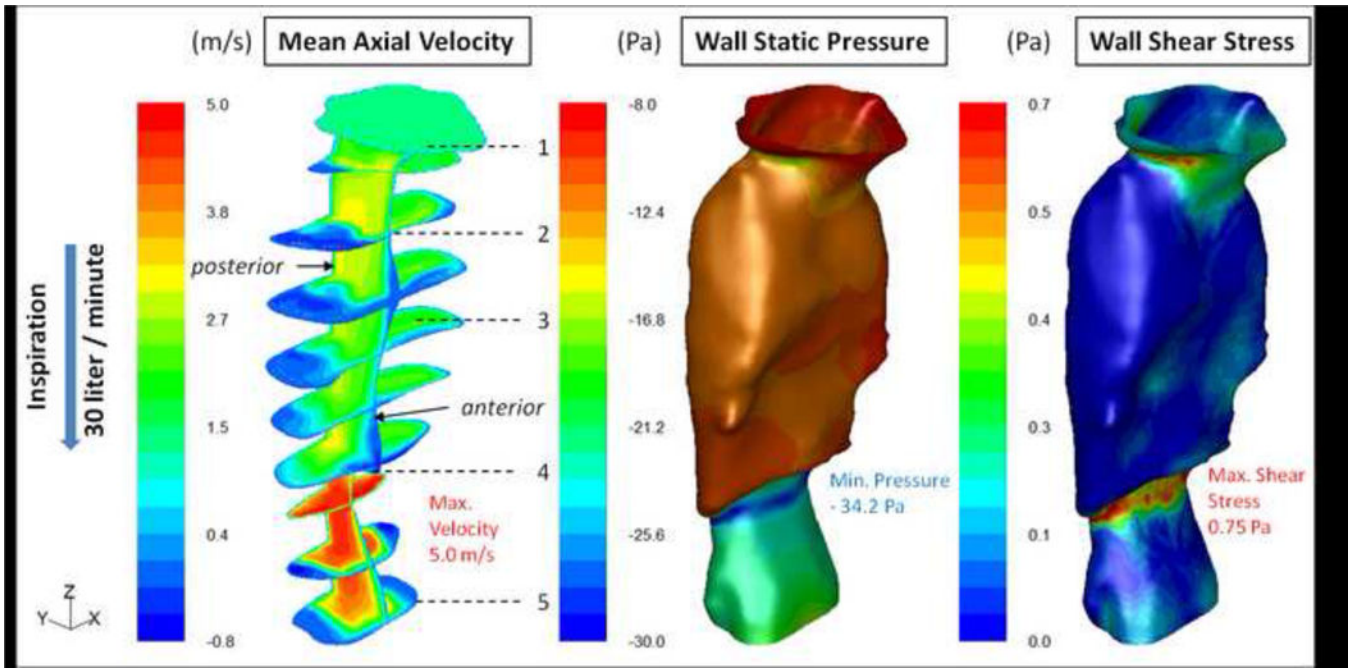

Figure 3.

SDB Patient #5: Post-treatment distributed contour values of mean axial velocity (m/sec), mean wall static pressure (Pa), and mean wall shear stress (Pa) as calculated with steady-state RANS (k-ω SST model) during inspiration. There is a more homogeneous distribution of the wall static pressure and wall shear stress values as compared with the pre-treatment case presented in Figure 2.

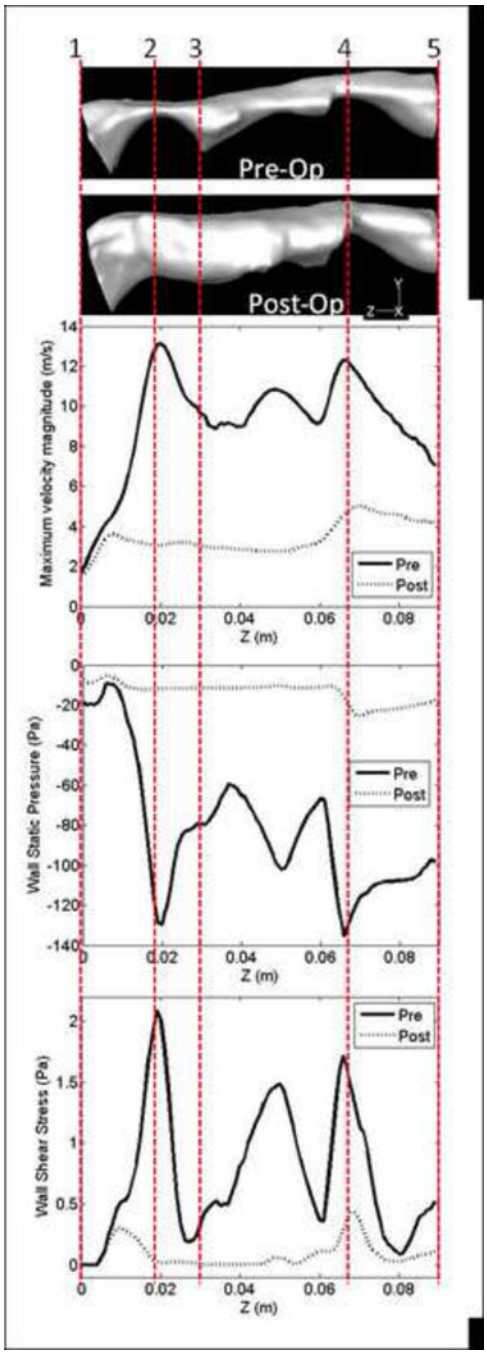

Figure 4.

SDB Patient #5: Comparison of flow variables along the pharyngeal airway during inspiration at pre and post-treatment conditions: maximum velocity magnitude (m/sec) along the airway; wall static pressure (Pa) distribution along the anterior airway wall in the mid-sagittal plane of the airway, and wall shear stress (Pa) distribution along the anterior airway wall in the mid-sagittal plane of the airway. Data obtained with steady-state RANS (k-ω SST model). The zones 1 to 5 (see also Figure 1) are marked on the horizontal side views of the pre and post-treatment pharyngeal airway models.

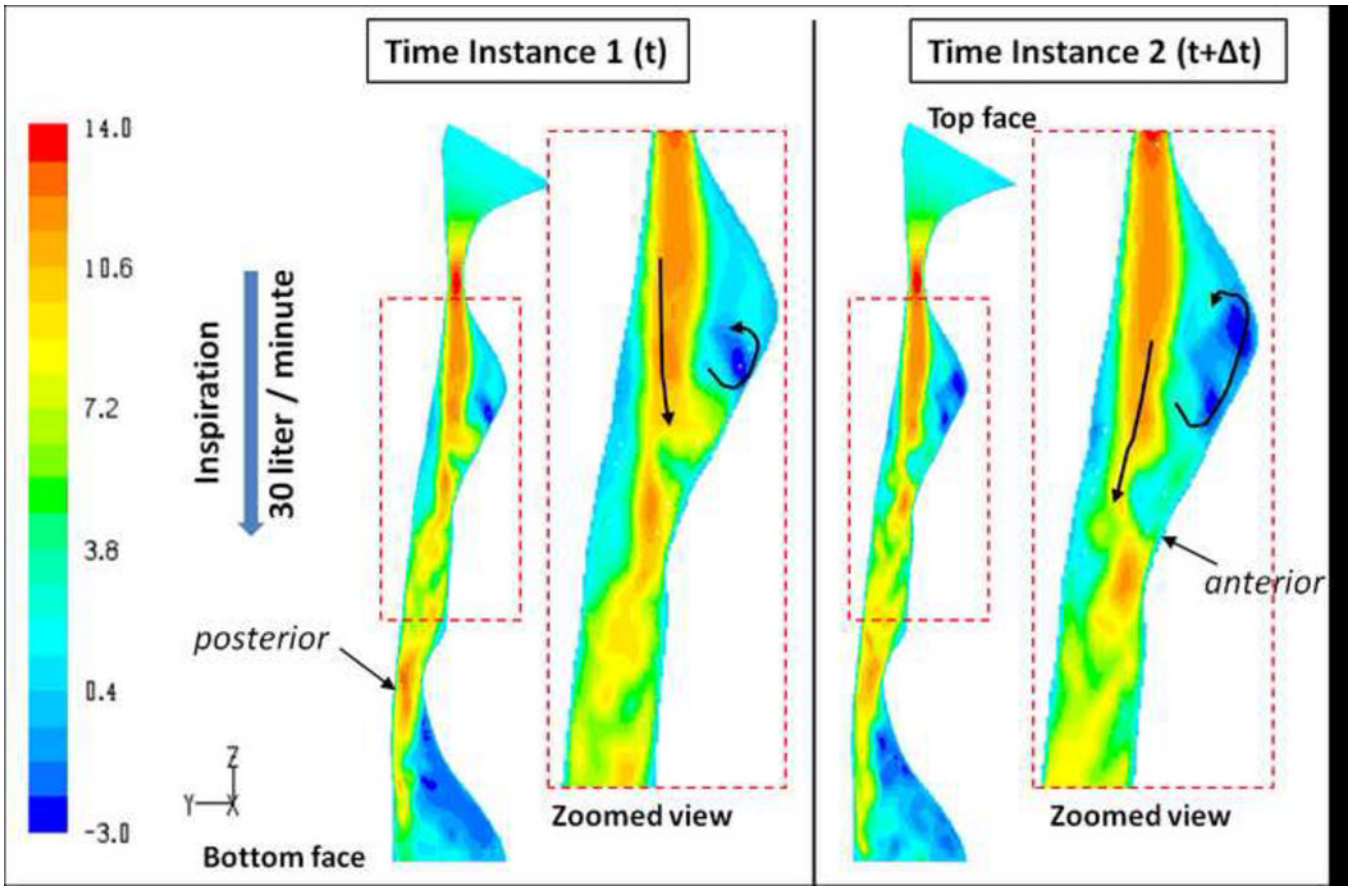

Figure 5.

SDB Patient #5: Pre-treatment instantaneous axial velocity distributions (m/sec) during inspiration along a sagittal plane through the airway model as calculated by unsteady LES. The data presented at two different time instances; the left two images compared to the right two images. Zoomed in views of the velocity field along the airway segment just downstream of the MCSA are shown for each time instance. The figure shows the dynamics of the flow in the airway from one time instance to another.

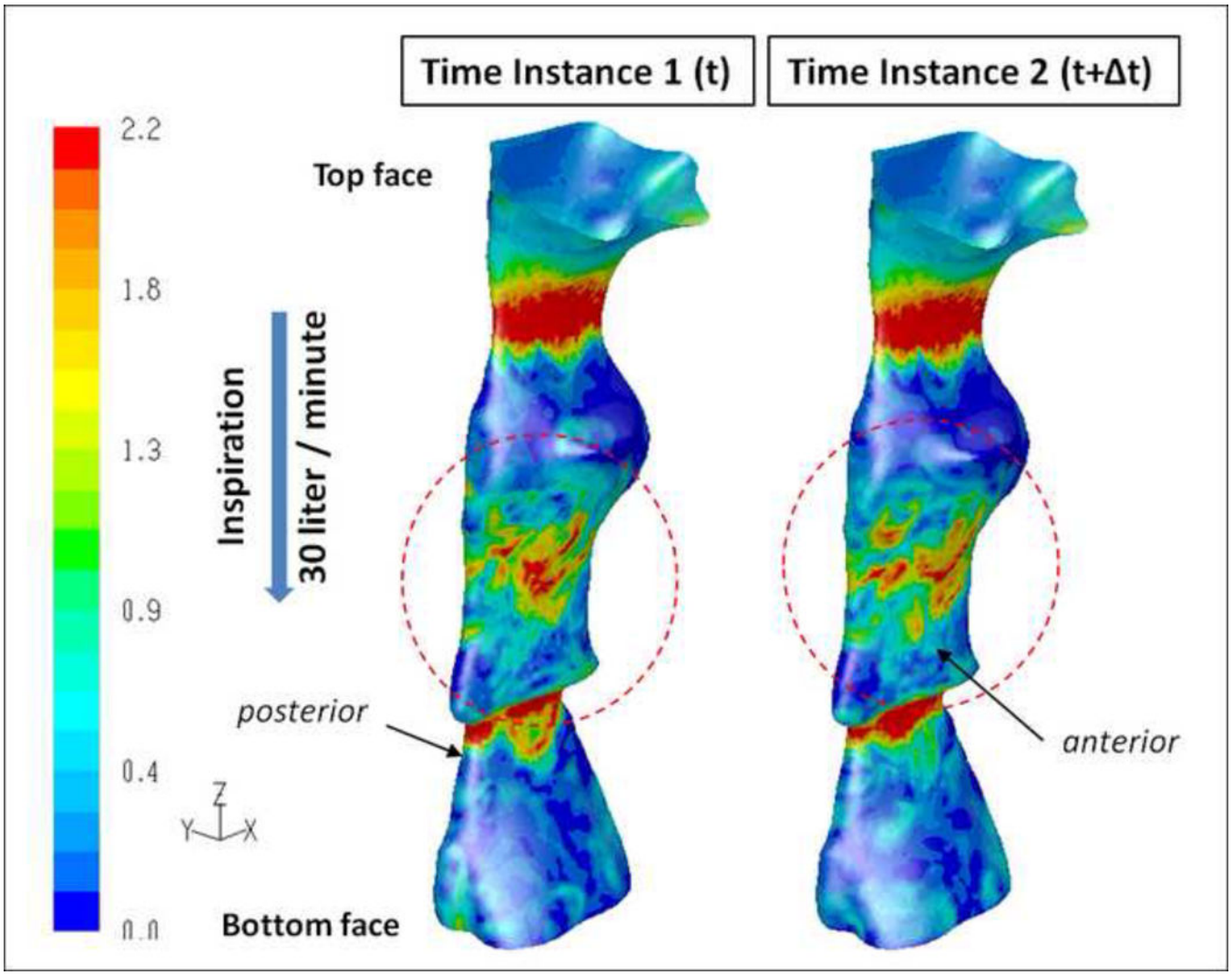

Figure 6.

SDB Patient #5: Pre-treatment instantaneous wall shear stress distributions (Pa) along the airway model as calculated by unsteady LES during inspiration. The data are presented at the same time instances shown in Figure 5. The data shows fluctuations in the wall shear stress values from one time step (left) to the other (right) in the jet impingement region on the anterior side of the airway wall.

Table 1

Cohort Characteristics: Demographics and Baseline Vitals

Subject	Treatment	Age (years)	Gender	Body Mass Index (kg/m^2)	Neck circumference (cm)	Blood Pressure (mmHg)	Epworth Sleepiness Scale	Snoring* (VAS)
1	Control	35	Female	24.3	33.0	101/64	0	0.0
2	Control	30	Female	19.0	29.2	100/60	2	0.7
3	Control	32	Male	34.0	41.0	128/87	0	0.0
4	Control	26	Male	27.3	42.0	126/80	3	0.0
5	MMA	37	Male	23.1	38.5	110/70	8	7.0
6	MMA	52	Male	29.4	42.0	130/70	10	8.4
7	PAP	56	Male	31.7	43.0	130/70	6	10
8	PAP	52	Male	24.4	40.5	120/82	14	7.2

BMI - body mass index (kg/m^2)

BP - blood pressure (mmHg)

BPM - beats per minute Neck size - in centimeters

*VAS-Visual Analog Scale (10cm)

*VAS Anchors (0 cm= no snoring, 10 cm=severe habitual snoring)

Table 2

Full night attended polysomnographic data at pre and post-treatment

Subject and treatment	Condition	TST (min)	SE (%)	Stage N3 (%)	REM (%)	AHI	BMI (kg/m^2)	Baseline Sats (%)	Nadir O_2 Sats (%)
5 MMA	pre	341	78	9.7	24.6	26.3	23.0	100	92
	post	374	79.5	16.4	16.3	4.3	22.1	100	91
6 MMA	pre	370	89	0.4	18.5	39.4	29.4	93	83
	post	280	89	4.6	29.1	10.5	28.1	92	89
7* PAP@9cmH_2O	pre	245	52.3	36.7	3.7	53.0	31.7	100	74
	post	354	90.3	6.6	21.2	1.8	31.7	100	93
8* PAP@8cmH_2O	pre	440	86.3	0.0	17	28.7	24.4	100	92
	post	432	88.8	0.6	2.7	11.4	24.4	100	92

TST - Total sleep time (minutes)

SE (%) - Sleep Efficiency

N3 - Delta sleep

REM - Rapid eye movement sleep

AHI - apnea hypopnea index

BMI - body mass index (kg/m^2)

Sats - oxyhemoglobin saturation;

MMA - maxillary-mandibular advancement

PAP - positive airway pressure.

*Each CPAP patient was tolerant and maintained the original titration listed (@ cm H_2O).

Table 3

Computational Fluid Dynamics summarized outputs for all subjects.

Subject	Maximum velocity (m/s)		Maximum Wall Shear Stress (Pa)		Minimum wall static pressure (Pa)		Airway resistance (Pa/Liter/minute)	
Controls	**Inspiration**	**Expiration**	**Inspiration**	**Expiration**	**Inspiration**	**Expiration**	**Inspiration**	**Expiration**
1	4.63	4.99	0.77	0.97	−10.5	−17.4	0.23	0.38
2	7.79	7.64	1.63	1.38	−28.9	−41.2	0.85	0.98
3	7.51	7.46	1.58	1.03	−33.5	−41.7	0.45	0.87
4	8.98	8.71	1.56	1.24	−42.3	−55.7	0.71	1.20
Mean±SD	7.2±1.9	7.2±1.6	1.4±0.4	1.2±0.2	−29±13	−39±16	0.56±0.28	0.86±0.35
Treated	Inspiration PRE / POST	Expiration PRE / POST	Inspiration PRE / POST	Expiration PRE / POST	Inspiration PRE / POST	Expiration PRE / POST	Inspiration PRE / POST	Expiration PRE / POST
5	13.3/5.0	14.5/5.3	2.5/0.75	2.84/0.7	−134/−9.0	−170/−23	2.7/0.41	2.51/0.35
6	16.2/2.52	21.4/3.1	4.84/0.23	5.52/0.34	−270/−2.7	−408/−4.4	4.47/0.09	5.98/0.07
7	17.4/5.04	19.24/4.5	5.21/0.25	5.54/0.6	−231/−9.0	−316/−8	3.97/0.15	3.34/0.40
8	26.4/12.8	24.7/12.5	6.5/2.29	5.45/2.26	−520/−125	−465/−120	6.16/1.72	5.4/1.80
Mean±SD	18.3±5.7 / 6.3±4.5	20.0±4.3 / 6.4±4.2	4.8±1.7 / 0.9±1.0	4.8±1.3 / 1.0±0.9	−289±164 / −36±59	−340±129 /−39±55	4.3±1.4 / 0.6±0.8	4.3±1.6 / 0.7±0.8
p-value[1]	0.73	0.72	0.39	0.71	0.82	0.99	0.9	0.66
p-value[2]	0.002	0.006	0.01	0.01	0.02	0.01	0.005	0.02

Pharyngeal airway flow data as predicted by CFD using the steady-state RANS model for non-SDB controls and for SDB patients at pre-and post-treatment conditions during both inspiratory and expiratory phases at the peak flow rate of 30L/min.

PRE – Pre-treatment, POST – Post-treatment

[1]Student's t-test to test the difference between non-SDB controls and treated post-treatment values. There was no statistical difference between controls and post-treatment values.

[2]Paired t-test to test the difference between pre-treatment and post-treatment values in the treated patients. There were statistically significant reductions in maximum velocity, maximum wall shear stress, minimum wall static pressure in the RP region, and airway resistance after treatment.

Table 4

Comparison of steady-state Reynolds Averaged Navier-Stokes and unsteady Large Eddy Simulation results.

CFD approach	Maximum velocity (m/s)		Maximum wall shear stress (Pa)		Minimum wall static pressure (Pa)		Airway resistance (Pa/Liter/minute)	
	Inspiration PRE / POST	Expiration PRE / POST	Inspiration PRE / POST	Expiration PRE / POST	Inspiration PRE / POST	Expiration PRE / POST	Inspiration PRE / POST	Expiration PRE / POST
RANS	13.3/5.0	14.5/5.3	2.5/0.75	2.84/0.70	−134/−9	−170/−23	2.70/0.41	2.51/0.35
LES	14.1/5.0	16.0/5.3	3.52/0.92	4.98/1.07	−159/−7	−231/−30	3.15/0.42	5.00/0.38

PRE – Pre-treatment; POST – Post-treatment; RANS – Reynolds Averaged Navier-Stokes model; LES – Large Eddy Simulation approach.

All values for subject #5, before and after treatment with maxillo-mandibular advancement.